Global sensitivity analysis of piezoelectric energy harvesters

Rabie Aloui, Walid Larbi, Mnaouar Chouchane

Global Sensitivity Analysis of Piezoelectric Energy Harvesters

Rabie Aloui[a,b,*], Walid Larbi[b,**], Mnaouar Chouchane[a]

[a] *Université de Monastir, École Nationale d'Ingénieurs de Monastir, Laboratoire de Génie Mécanique, LA-MA-05, Monastir, Tunisia*
[b] *Structural Mechanics and Coupled Systems Laboratory (LMSSC), Conservatoire National des Arts et Métiers (CNAM), Paris, France*

Abstract

Vibration energy harvesting using the direct effect of piezoelectricity has attracted increasing attention during the last two decades. Different modeling techniques have been applied to describe the electromechanical coupling effect of a piezoelectric harvester and to predict its electrical output. This study aims to identify the most important properties of both harvester substrate material and piezoelectric material that cause uncertainty in the predicted performances of the harvester. Global sensitivity analysis, applied in this paper, is a promising method used to identify systems parameters which have significant impact on the system output. In this paper, the Elementary Effects method (EEs), a particular implementation of the global sensitivity method, is used to identify the impact of substrate and piezoelectric material properties on the voltage frequency response function of a typical bimorph piezoelectric energy harvester with fixed geometry. With a small number of model evaluations at selected ranges of material properties,

* Corresponding author
** Principal corresponding author
Email addresses: rabie.aloui@enim.rnu.tn (Rabie Aloui), walid.larbi@cnam.fr (Walid Larbi), mnaouar.chouchane@enim.rnu.tn (Mnaouar Chouchane)

it has been found that the elastic modulus and density of the piezoelectric layer are the parameters which lead to the largest output variability. Furthermore, it has been found that the order of importance of the parameters can change from short-circuit to open-circuit conditions.
Keywords: Global Sensitivity Analysis, Elementary Effects, Piezoelectric Energy Harvesting, Finite Element Method

1. Introduction

Energy harvesting using piezoelectric material has attracted considerable interest in the last decade. Piezoelectric material displays converting capabilities due to its direct and indirect electromechanical effect. Several approaches have been developed to model Piezoelectric Energy Harvesters (PEHs). In particular, two methods have been accepted and are the most widely used in the scientific community: (i) the analytical distributed parameter model introduced by Erturk and Inman [1, 2] is applied for unimorph and bimorph harvesters to obtain a modal solution of second-order ordinary differential equations, (ii) the finite element method, adapted by De Marqui Junior et al. [3, 4], uses standard discretization to provide discrete models with less restrictive assumptions on the global electrical variables. The two modeling approaches are particularly useful as they have been amply tested showing close correlation with experimental data.

In the frame of numerical approaches, sensitivity analysis is a very useful tool for modeling and design analysis of mechatronic systems. It is applied in various engineering problems such as structural analysis, model updating, design optimization of structures, system control and uncertainty propagation [5]. Sensitivity analysis enables the evaluation of the degree of influence

of input parameters on the output responses of the modeled system. Furthermore, this method process is widely considered as the most important step in design optimization since significant number of optimization algorithms require the prediction of the evolution of the output responses of the system for different values of design variables [6].

Sensitivity analysis techniques can be classified into local and global methods. Local sensitivity analysis, often referred to as a one factor at time analysis, is based on the approximation of partial derivatives to assess how uncertainty in one factor affects the model response keeping other factors fixed at their nominal values. Global Sensitivity Analysis (GSA), on the other hand, offers a comprehensive approach to the studied model, since it evaluates the effect of factors that are varying within the considered multi-dimensional input space [7].

In recent published research, Sharp and Brooks [8] introduced expressions for the sensitivities of the Frequency Response Functions (FRFs) of linear constant coefficient systems with distinct eigenvalues to perturbations of the design parameters suggesting several engineering applications of the developed theory. Lasecka-Plura et al [5] studied the sensitivity of the FRF and steady-state vibration response of planar frames with viscoelastic dampers. A comparison was made between the first-order, the second-order and the exact solution sensitivities. Analysis show that the second order sensitivity gives results which are very close to the exact solution, when the perturbation of the parameter is smaller than 20%. Lima et al [6, 9] investigated the first order sensitivity of complex frequency response functions for composite sandwich plates composed of a combination of fiber-reinforced and elastomeric viscoelastic layers, frequently used for noise and vibration attenuation. The study aims to find the sensitivity of viscoelastic struc-

tures to variation of temperature and structural parameters. Ng and Liao [10] used the first order sensitivity to evaluate the performances of sensing and power generation of the piezoelectric energy harvesters to variation of elastic substrate properties for three type of sensors. The reported research results show that for the series bimorph piezoelectric sensor, the voltage sensitivity is the highest and the charge sensitivity is the lowest. For the parallel bimorph piezoelectric sensor, the voltage sensitivity is the lowest and charge sensitivity is highest. A unimorph sensor, however, has relatively medium sensitivities of charge and voltage responses. Ruiz et al [11] analyzed the uncertainty propagation and global sensitivity of the FRFs of the output voltage of piezoelectric energy harvesters. Their approach is based on the identification of Sobol' indices to assess the robustness of the stochastic prediction. Peralta et al [12] introduced a procedure to update the electromechanical properties of the PEHs based on Bayesian updating techniques and global sensitivity analysis. The introduced approach constitutes a powerful method for the robust design and prediction of the performances of piezoelectric energy harvesters.

In the literature, several GSA methods are applied [13, 14, 15] ranging from qualitative screening techniques [16, 17] to quantitative methods based on variance decomposition [18, 19]. The Morris method [16] is a global sensitivity screening technique used to derive sensitivity measures from a set of local derivatives sampled on a grid throughout the parameter space [20]. This technique investigates the model response to a change in the inputs by varying One-At-a-Time (OAT), while keeping all other variables fixed. The local sensitivity measure associated to each factor is called elementary effect and is defined as the ratio between the variation in the model response output and the variation in the input factor. In order to obtain a global

sensitivity measure, different elementary effects (local derivatives taken at points sampled throughout the parameter space) for each parameter are estimated and averaged. Two sensitivity measures are carried out, the first one is the *mean* of the EEs which is refined by Campolongo et al [7, 21] consisting in averaging the absolute values of the elementary effects. The second measure is the *standard deviation* of the EEs. By plotting both sensitivity measures, the Morris method identifies the hierarchical order of influence of the input parameters on the model output.

Most of the previous researches were limited to local sensitivities for variation of system parameters in the vicinity of the considered nominal configuration. Generally, an interval variation of system parameter is more acceptable than a nominal parameter, hence the importance of applying global sensitivity. Morris method computes global sensitivity in an efficient way. Previously published research work does not seem to have applied this method in sensitivity analysis of piezoelectric harvesters. In this paper, we propose combining the implementation of the PEH model with Morris elementary effect estimation method to determine the effect of uncertain electromechanical parameters of a bimorph piezoelectric energy harvester on the output voltage for short-circuit and open-circuit conditions. Furthermore, the effective electromechanical coupling factor is monitored for the model evaluations used to compute elementary effects. In order to predict the output voltage of the studied harvester, a finite element formulation of a laminated piezoelectric harvester is applied. The mathematical development of the model is given in Section 2. This model is used in Section 3 to derive the complex FRFs of a bimorph piezoelectric energy harvester considered as a case study in this paper. In Section 4, the Morris method is applied using the modulus of the voltage FRF of the harvester as an output and

a set of uncertain physical parameters. The considered numerical example presented in Section 5 shows the robustness of the EEs method compared to others GSA methods. Furthemore, the global sensitivities of the voltage FRF of a bimorph piezoelectric harvester based on elementary effects have been compared with those computed using the variance decomposition based sensitivity analysis method described in reference [11] for different configurations of the PEHs.

2. Finite Element Modeling of a Piezoelectric Composite Beam

Considering a laminated piezoelastic beam composed of K layers including P piezoelectric layers excited under base motion at the clamped end as shown in Figure 1. In the absence of mechanical dissipative effects, the extended Hamilton's principle for an electromechanical body, between the two known times t_1 and t_2, is [22]:

$$\int_{t_1}^{t_2} (\delta T - \delta U + \delta W_{nc}) dt = 0 \tag{1}$$

where δT is the first variation of the kinetic energy, δU is the first variation of the internal energy including the piezoelectric effect contribution and δW_{nc} is the virtual work done by the non-conservative electric charge components.

The thin piezoelectric layers of the cantilever beam are poled in the thickness direction with an electrical field applied parallel to this polarization direction. Such a configuration is characterized in particular by the electromechanical coupling between the axial strain and the transverse electrical field [23]. The reduced constitutive equations corresponding to the p^{th} piezoelectric layer is written as follows, $p \in \{1, \cdots, P\}$:

$$\sigma_1^{(p)} = \overline{c}_{11}^{(p)} \varepsilon_1^{(p)} - \overline{e}_{31}^{(p)} E_3^{(p)} \tag{2}$$

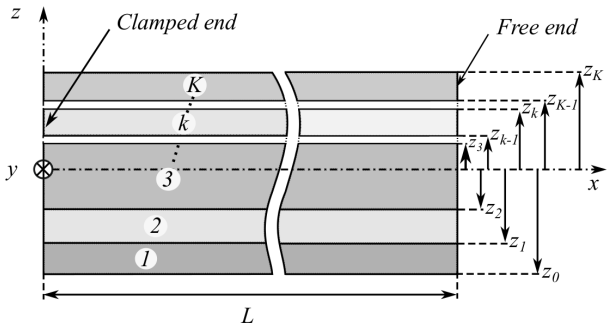

Figure 1: A multilayer piezoelectric cantilever beam: $k \in \{1, \cdots, K\}$

$$D_3^{(p)} = \overline{e}_{31}^{(p)} \varepsilon_1^{(p)} + \overline{\epsilon}_{33}^{(p)} E_3^{(p)} \tag{3}$$

where $\sigma_1^{(p)}$, $\varepsilon_1^{(p)}$, $E_3^{(p)}$ and $D_3^{(p)}$ are respectively the normal stress, the normal strain, the electric field and the electric displacement; $\overline{c}_{11}^{(p)}$ is the elastic modulus, $\overline{e}_{31}^{(p)}$ is the piezoelectric coupling coefficient and $\overline{\epsilon}_{33}^{(p)}$ is the permittivity at constant strain. The electric field $E_3^{(p)}$ is normal to the electrodes of the piezoelectric layer and its intensity is assumed to be uniform in the piezoelectric thickness direction. The superscript (p) refers to the piezoelectric material. Moreover, the thickness of the electrodes is much smaller than the thickness of piezoelectric layer so that the equipotentiality assumption in the piezoelectric electrodes is well satisfied. Thus the electric field can be expressed as:

$$E_3^{(p)} = -\frac{V^{(p)}}{h^{(p)}} \tag{4}$$

where $V^{(p)}$ is the potential difference between the upper and the lower electrode surfaces and $h^{(p)} = z_p - z_{p-1}$ is the thickness of the p^{th} piezoelectric layer.

The equations of the coupled electromechanical variational formulation

can be rewritten in the following form [23, 24]:

$$\sum_{k=1}^{K}\int_{\Omega^k}\rho^k\left(\ddot{u}_x\delta u_x+\ddot{u}_z\delta u_z\right)d\Omega+\sum_{k=1}^{K}\int_{\Omega^k}\bar{c}_{11}^{k}\varepsilon_1\delta\varepsilon_1 d\Omega+\sum_{p=1}^{P}\frac{V^{(p)}}{h^{(p)}}\int_{\Omega^{(p)}}\bar{e}_{31}^{(p)}\delta\varepsilon_1 d\Omega=0 \tag{5}$$

$$-\sum_{p=1}^{P}\frac{\delta V^{(p)}}{h^{(p)}}\int_{\Omega^{(p)}}\bar{e}_{31}^{(p)}\varepsilon_1 d\Omega+\sum_{p=1}^{P}\frac{\delta V^{(p)}}{h^{(p)}}\int_{\Omega^{(p)}}\bar{\epsilon}_{33}^{(p)}\frac{V^{(p)}}{h^{(p)}}d\Omega+\sum_{p=1}^{P}\delta V^{(p)}Q^{(p)}=0 \tag{6}$$

where ρ^k and Ω^k are respectively the mass density and the domain occupied by the k^{th} layer, and $Q^{(p)}$ is the electrical charge of the p^{th} piezoelectric layer. Furthermore, the mechanical displacements fields u_x and u_z of the laminated harvester under base excitation, based on Euler-Bernoulli beam assumptions, are defined as follow:

$$u_x(x,z,t)=u(x,t)-z\theta(x,t) \tag{7}$$

$$u_z(x,z,t)=w(x,t)=w_b(t)+w_{rel}(x,t) \tag{8}$$

where u is the axial displacement of the center line of the beam, $\theta = \partial w_{rel}/\partial x$ is the beam section rotation, w is the transverse displacement, $w_b(t)=w_b e^{j\omega t}$ is the base displacement and w_{rel} is the relative transverse displacement of clamped-free beam.

Applying the finite element method, the previous formulations uses a standard discretization of N mechanical Degrees Of Freedom (DOFs) and provides less restrictive assumptions on the electrical DOFs: only one electrical DOF for each piezoelectric layer is needed due to the equipotentiality in the electrodes. In this paper, three mechanical degrees of freedom per node are assumed ($u,\ w,\ \theta$). Details of the stratified beam finite element discretization are provided in [23] for the master element shape functions. The various terms appearing in the variational formulation of Equations (5)

and (6) in terms of Hamilton's principle are now discussed. The discrete form for each term is provided [22]:

(i) The kinetic energy variation is:

$$\delta T = -\sum_{k=1}^{K} \int_{\Omega^k} \rho^k \left(\ddot{u}_x \delta u_x + \ddot{u}_z \delta u_z \right) d\Omega \Rightarrow -\delta \mathbf{U}^T \mathbf{M}_m \ddot{\mathbf{U}}(t) + \delta \mathbf{U}^T \mathbf{F}(t) \quad (9)$$

where $\mathbf{M}_m$ is the global $(N \times N)$ mass matrix, $\mathbf{U}(t) = \mathbf{U}e^{j\omega t}$ is the global $(N \times 1)$ vector of mechanical coordinates displacements, $\mathbf{F}(t) = \mathbf{F}e^{j\omega t}$ is the global $(N \times 1)$ forcing vector due to base excitation, which can be expressed as an $(N \times 1)$ effective mass vector $\mathbf{m}^*$ multiplied by the base acceleration [3, 22] as follows:

$$-\sum_{k=1}^{K} \int_{\Omega^k} \rho^k \delta w_{rel} \ddot{w}_b d\Omega \Rightarrow \delta \mathbf{U}^T \mathbf{m}^* \ddot{w}_b(t) = \delta \mathbf{U}^T \mathbf{F}(t) \quad (10)$$

(ii) The internal energy variation is:

$$\begin{aligned} \delta U = &\sum_{k=1}^{K} \int_{\Omega^k} \overline{c}_{11}^k \varepsilon_1 \delta \varepsilon_1 d\Omega + \sum_{p=1}^{P} \frac{V^{(p)}}{h^{(p)}} \int_{\Omega^{(p)}} \overline{e}_{31}^{(p)} \delta \varepsilon_1 d\Omega \\ &+ \sum_{k=1}^{P} \frac{\delta V^{(p)}}{h^{(p)}} \int_{\Omega^{(p)}} \overline{e}_{31}^{(p)} \varepsilon_1 d\Omega - \sum_{k=1}^{K} \frac{\delta V^{(p)}}{h^{(p)}} \int_{\Omega^{(p)}} \overline{\epsilon}_{33}^{(p)} \frac{V^{(p)}}{h^{(p)}} d\Omega \end{aligned} \quad (11)$$

- The first term of Equation (11) is the mechanical contribution to the internal energy variation:

$$\sum_{k=1}^{K} \int_{\Omega^k} \overline{c}_{11}^k \varepsilon_1 \delta \varepsilon_1 d\Omega \Rightarrow \delta \mathbf{U}^T \mathbf{K}_m \mathbf{U}(t) \quad (12)$$

  where $\mathbf{K}_m$ is the global $(N \times N)$ stiffness matrix.

- The second and third terms in Equation (11) are the piezoelectric contributions to the internal energy variation related to the direct and inverse effects:

$$\sum_{p=1}^{P} \frac{V^{(p)}}{h^{(p)}} \int_{\Omega^{(p)}} \overline{e}_{31}^{(p)} \delta \varepsilon_1 d\Omega \Rightarrow \delta \mathbf{U}^T \mathbf{K}_c \mathbf{V}(t) \quad (13)$$

$$\sum_{k=1}^{P} \frac{\delta V^{(p)}}{h^{(p)}} \int_{\Omega^{(p)}} \overline{e}_{31}^{(p)} \varepsilon_1 d\Omega \Rightarrow \delta \mathbf{V}^T \mathbf{K}_c^T \mathbf{U}(t) \tag{14}$$

where $\mathbf{K}_c = (\mathbf{K}_c^{(1)} \cdots \mathbf{K}_c^{(P)})$ is the global $(N \times P)$ electromechanical coupling matrix, $\mathbf{V}(t) = \mathbf{V}e^{j\omega t}$ is the global $(P \times 1)$ vector of voltage outputs.

- The last term in Equation (11) is the electrostatic contribution to the internal energy variation is:

$$\sum_{k=1}^{K} \frac{\delta V^{(p)}}{h^{(p)}} \int_{\Omega^{(p)}} \epsilon_{33}^{(p)} \frac{V^{(p)}}{h^{(p)}} d\Omega \Rightarrow \delta \mathbf{V}^T \mathbf{K}_e \mathbf{V}(t) \tag{15}$$

where $\mathbf{K}_e = diag(C^{(1)} \cdots C^{(P)})$ is the diagonal global $(P \times P)$ capacitance matrix, and $C^{(p)} = \dfrac{b \times L}{h^{(p)}} \overline{\epsilon}_{33}^{(p)}$ is the capacitance of the p^{th} piezoelectric layer.

(iii) The variation of work due to the charges is:

$$\delta W_{nc} = \sum_{p=1}^{P} \delta V^{(p)} Q^{(p)} \Rightarrow \delta \mathbf{V}^T \mathbf{Q}(t) \tag{16}$$

where $\mathbf{Q}(t) = \mathbf{Q}e^{j\omega t}$ is the global $(P \times 1)$ vector of electric charge outputs. The harvested energy is dissipated through a resistive electrical load R. Using Ohm's law, the following additional equation relates the voltage vector $\mathbf{V}$ to the time derivative of the charge vector $\mathbf{Q}$:

$$\mathbf{V}(t) = R\dot{\mathbf{Q}}(t) \tag{17}$$

To account for system damping, a proportional viscous damping is assumed and included in the model. The global $(N \times N)$ damping matrix $\mathbf{C}_m$ is assumed to be a linear combination of the mass and stiffness matrices (the Rayleigh damping), so that:

$$\mathbf{C}_m = \alpha \mathbf{M}_m + \beta \mathbf{K}_m \tag{18}$$

where α and β are real proportional coefficients which are typically determined from the measurement of modal damping.

The general damped electromechanical equations obtained from the previous finite element formulation can be expressed as [25, 26, 27]:

$$\mathbf{M}_m\ddot{\mathbf{U}}(t) + \mathbf{C}_m\dot{\mathbf{U}}(t) + \mathbf{K}_m\mathbf{U}(t) + \mathbf{K}_c\mathbf{V}(t) = \mathbf{F}(t) \tag{19}$$

$$\mathbf{K}_e\mathbf{V}(t) - \mathbf{K}_c^T\mathbf{U}(t) + \mathbf{Q}(t) = 0 \tag{20}$$

where Equation (19) corresponding to the mechanical equation of motion includes the inverse effect electromechanical coupling term, whereas Equation (20) corresponding to the electrical equation includes the direct effect electromechanical coupling term introduced by the piezoelectric behavior.

2.1. Natural frequencies of the harvester for the short-circuit and the open-circuit conditions

The natural frequencies of the harvester are calculated by solving the free undamped system corresponding to Equation (19). For piezoelectric energy harvesters, two natural frequencies are defined as a characteristic limit bounds for each vibration mode: *(i)* the short-circuit natural frequencies are calculated by assuming that no potential difference exists across the piezoelectric layers in free vibration. As a result, the electromechanical coupling in Equation (19) is omitted, *(ii)* the open circuit natural frequencies, however, are calculated by assuming that no charge flows in the electrical circuit [28]. In practice, these natural frequencies are determined in terms of the load resistance value. The short-circuit condition corresponds to a low resistive load connected to the electrodes of the piezoelectric layers ($R \to 0$), whereas the open-circuit condition is determined for a high load resistance ($R \to \infty$). The main motivation of computing these particular limits is

to determine the electromechanical coupling factor, using a classical elastic mechanical formulation, which corresponds to the electromechanical energy ratio.

The normal modes of the short-circuit system are obtained assuming harmonic solutions of the undamped equations of motion (19) for $\mathbf{V} = \mathbf{0}$ and $\mathbf{F} = \mathbf{0}$.

$$\left[\mathbf{K}_m - \omega_i^2 \mathbf{M}_m\right] \mathbf{\Phi}_i = \mathbf{0} \tag{21}$$

where ω_i is the natural frequency and $\mathbf{\Phi}_i$ is eigenvector for the i^{th} mode for short-circuit condition. These modes verify the following orthogonality properties:

$$\mathbf{\Phi}_i^T \mathbf{M}_m \mathbf{\Phi}_j = \delta_{ij} \quad \text{and} \quad \mathbf{\Phi}_i^T \mathbf{K}_m \mathbf{\Phi}_j = \omega_i^2 \delta_{ij} \tag{22}$$

where δ_{ij} is the Kronecker symbol and the mode $\mathbf{\Phi}_i$ is normalized with respect to the structural mass matrix.

The eigenvalue problem for the open-circuit condition is derived by coupling Equations (19) and (20) substituting $\mathbf{Q} = \mathbf{0}$ and $\mathbf{F} = \mathbf{0}$:

$$\left[\widehat{\mathbf{K}}_m - \widehat{\omega}_i^2 \mathbf{M}_m\right] \widehat{\mathbf{\Phi}}_i = \mathbf{0} \tag{23}$$

where $\widehat{\mathbf{K}}_m = \mathbf{K}_m + \mathbf{K}_c \mathbf{K}_e^{-1} \mathbf{K}_c^T$ is the stiffness matrix for the open-circuit condition which depends on the piezoelectric system properties, $\widehat{\omega}_i$ is the natural frequency and $\widehat{\mathbf{\Phi}}_i$ is eigenvector for the i^{th} vibration mode. These modes verify the following orthogonality properties:

$$\widehat{\mathbf{\Phi}}_i^T \mathbf{M}_m \widehat{\mathbf{\Phi}}_j = \delta_{ij} \quad \text{and} \quad \widehat{\mathbf{\Phi}}_i^T \widehat{\mathbf{K}}_m \widehat{\mathbf{\Phi}}_j = \widehat{\omega}_i^2 \delta_{ij} \tag{24}$$

2.2. Effective Electromechanical Coupling Factor

The dimensionless Effective Electromechanical Coupling Factor (EEMCF) of the piezoelectric laminated beam for the i^{th} mode can be expressed in

terms of the natural frequencies of the short and open-circuit conditions. This factor defines the exchange of energies of the vibrating structure at the i^{th} mode. It is usually defined, as follows [29, 30, 31]:

$$k^2_{eff,i} = \frac{\widehat{\omega}_i^2 - {\omega_i}^2}{{\omega_i}^2} \tag{25}$$

3. The Bimorph Piezoelectric Energy Harvester

The finite element formulation, presented in Section 2, can be easily adapted to the case of a bimorph piezoelectric energy harvester considered as a case study in this paper. The harvester is composed of two identical piezoelectric layers, so that $P = 2$ and $C^{(1)} = C^{(2)} = C$, bonded to an elastic substrate beam as shown in Figure 2. Thus, the harvester has a total of three layers ($K = 3$). The harvester is assumed to be a linear input-output system which is characterized by its Frequency Response Functions.

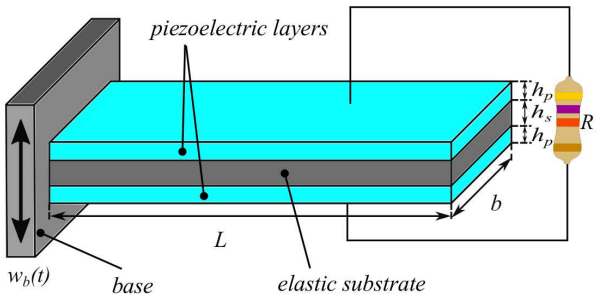

Figure 2: A Clamped free bimorph piezoelectric energy harvester under base excitation with a load resistance mounted in series

The FRFs are defined here as the output responses of the harvester (displacement or voltage) per base acceleration versus the excitation frequency.

Transforming Equations (19) and (20) to the frequency domain, the equivalent expression for nodal displacements FRFs relative to the electrical configurations (load resistance mounted in series or parallel connection) is given in the following equation in which the electrical DOFs are eliminated [32, 33].

$$\frac{\mathbf{U}}{-\omega^2 w_b} = \left[-\omega^2 \mathbf{M}_m + j\omega \mathbf{C}_m + \mathbf{K}_m + \frac{j\omega\ \mathbf{K}_c^{eq}\ \mathbf{K}_c^{eqT}}{\left(\frac{1}{R} + j\omega C^{eq}\right)} \right]^{-1} \mathbf{m}^* \tag{26}$$

where $\mathbf{K}_c^{eq}$ and C^{eq} are respectively the equivalent electromechanical coupling vector and the equivalent capacitance for a series and parallel connections of the load resistance with piezoelectric layers [33], which are given in Table 1. For the mechanical vibration response, only the transverse tip displacement FRF $\left(\frac{w_n}{-\omega^2 w_b}\right)$ is considered in this study. The index $n = N/3$ is the total number of nodes used to discretize the beam harvester with linear elements.

Table 1: Equivalent terms of a bimorph energy harvester for the series and the parallel connections of the piezoceramic layers

Terms	Series connection	Parallel connection
$\mathbf{K}_c^{eq}$	$\frac{\mathbf{K}_c^{(1)} + \mathbf{K}_c^{(2)}}{2}$	$\mathbf{K}_c^{(1)} + \mathbf{K}_c^{(2)}$
C^{eq}	$\frac{C}{2}$	$2C$

Similarly, for the electrical outputs, the resultant voltage FRF of the harvester is obtained as a function of the nodal displacements FRFs as follows [32]:

$$\frac{V}{-\omega^2 w_b} = \frac{j\omega\ \mathbf{K}_c^{eqT}}{\left(\frac{1}{R} + j\omega C_p^{eq}\right)} \left(\frac{\mathbf{U}}{-\omega^2 w_b}\right) \tag{27}$$

The current I and the electrical power P FRFs are derived from the

voltage FRF:

$$\frac{I}{-\omega^2 w_b} = \frac{1}{R}\left(\frac{V}{-\omega^2 w_b}\right) \tag{28}$$

$$\frac{P}{(-\omega^2 w_b)^2} = \frac{1}{R}\left(\frac{V}{-\omega^2 w_b}\right)^2 \tag{29}$$

The global finite element matrices appearing in the frequency response functions Equations (26) and (27) establish the dependence of the response of the system on a set of parameters representing the physical characteristics of the harvester structure. In general, we assume that any complex frequency response function H of the BPEH can be expressed in the following form:

$$H = H\left(\omega, \boldsymbol{\theta}\right) \tag{30}$$

where $\boldsymbol{\theta}$ is a vector of physical parameters of the harvester.

4. Global Sensitivity Analysis of the Frequency Response Functions

4.1. The Elementary Effects Method

The Elementary Effects Method constitutes a simple way for screening the effect on the output responses of a few important input factors among the many factors that can be contained in the studied model. The fundamental idea behind this method is given by Morris [16, 34], who introduced the concept of elementary effects, proposing the construction of two sensitivity measures: the *mean* and the *standard deviation* of the EEs for each input parameter. In practice, this method is conducted by: (a) defining the model and its input parameters, (b) assigning Probability Density Function (PDF) to each input parameter, (c) generating an input matrix using an appropriate random sampling method, (d) calculating the corresponding output response

vector, and (e) computing the EEs and then the sensitivity measures of each input/output relationship [35]. The average and standard deviation are then computed for a set of elementary effects for each factor. The main goal is to determine which input factors could be considered to have effects which are [16, 17]:

1. Negligible (low mean, low standard deviation).
2. Linear and additive (high mean, low standard deviation).
3. Nonlinear or involved in interactions with other factors (high standard deviation).

This method computes the sensitivities of the outputs considering one factor at time among the input factors through the concept of EEs, which are approximations of the first order partial derivatives of the response. These elementary effects are estimated at a set of sampled points in the input space.

The finite element model of the bimorph piezoelectric energy harvester defined in Equations (26) and (27), is the model-parameters considered. The frequency response function H in Equation (30) is the model-output and the k independent parameters in vector $\boldsymbol{\theta}$ are the model-inputs. Each parameter θ_i is assumed to be scaled to take on values in the interval $[0, 1]$ as follows:

$$\overline{\theta}_i = \frac{\theta_i - \theta_{i,min}}{\theta_{i,max} - \theta_{i,min}} \tag{31}$$

where $\theta_{i,max}$ and $\theta_{i,min}$ are respectively the maximum and minimum bounds of the i^{th} parameter. The bar is omitted below to simplifying the notation. Thus, these non-dimensional parameters are randomly selected in a k-dimensional unit hypercube.

A discretized approach of the input space is proposed. In fact, the possible input values will be restricted to an experimental design, which is a

regular k-dimensional p-levels grid, where each θ_i may take a value from the set $\{0, 1/(p-1), 2/(p-1), \cdots, 1\}$. For a given vector $\boldsymbol{\theta}$, the elementary effect of the i^{th} input parameter is defined as follows [36, 16]:

$$EE_i(\boldsymbol{\theta}) = \frac{|H(\theta_i + \Delta, \boldsymbol{\theta}_{\sim i})| - |H(\boldsymbol{\theta})|}{\Delta} \tag{32}$$

where $|.|$ is the modulus, θ_i varies between 0 and $(1-\Delta)$; Δ is the variation size which is a predetermined multiple of $1/(p-1)$, and $\boldsymbol{\theta}_{\sim i}$ is the set of all parameters except the i^{th} parameter. The originality of the elementary effects method is based on selecting a set of r trajectories where parameters are changed one at a time on the design grid [7]. A trajectory enables the calculation of an elementary effect for each input parameter i between two points of the trajectory ($\boldsymbol{\theta}^{(j)}$ and $\boldsymbol{\theta}^{(j+1)}$, where $j \in \{1, .., k\}$) [17, 37]. Therefore, each trajectory requires $(k+1)$ model evaluations (simulations) to calculate k elementary effects (one EE per parameter).

Figure 3 presents a trajectory in a 3-dimensional space which is composed of a four sampling points $\{\boldsymbol{\theta}^{(1)}, \cdots, \boldsymbol{\theta}^{(4)}\}$ and $\Delta = 0.25$. Along a trajectory each input parameter is increased or decreased by the same step Δ. Considering, for example, the third component θ_3. This components differs only in the two consecutive sample points $\boldsymbol{\theta}^{(3)}$ and $\boldsymbol{\theta}^{(4)}$, thus:

$$EE_3 = \frac{|H(\boldsymbol{\theta}_4)| - |H(\boldsymbol{\theta}_3)|}{0.25} \tag{33}$$

A set of r different trajectories (with index t, where $t = 1, .., r$) provides r estimates of elementary effects related to each input parameter i, at the cost of $r \times (k+1)$ simulations.

The first measure of sensitivity is the average of the elementary effects

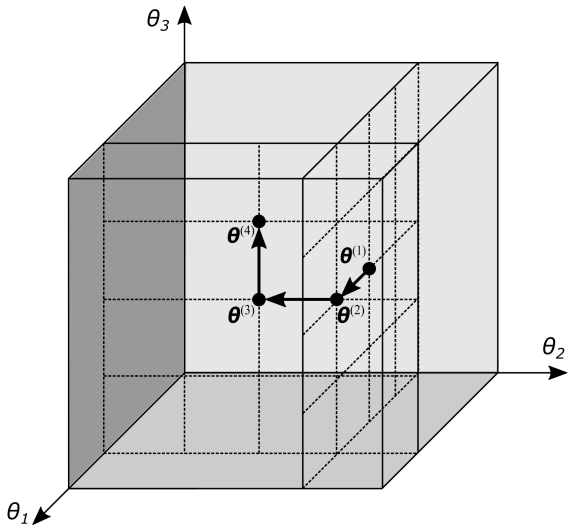

Figure 3: An example of a trajectory in the input domain for $k = 3$ and $p = 5$

which is computed for each input parameter i:

$$\mu_i = \frac{1}{r} \sum_{t=1}^{r} EE_i^{*(t)} \tag{34}$$

where $EE_i^{*(t)}$ is the normalized elementary effects of $EE_i^{(t)}$. This measure has been rectified by Campolongo et al. [21], who has recommended the use of the mean of absolute elementary effects, defined in Equation (32), rather than the usual average, since some EEs can eliminate each other in non-monotonic models. Thus, the mean of the absolute values of EEs is:

$$\mu_i^* = \frac{1}{r} \sum_{t=1}^{r} |EE_i^{*(t)}| \tag{35}$$

For a given parameter i, if the r estimates of EEs have the same sign, that means that this parameter has a monotonic effect on the output response, increasing or decreasing, depending on the sign of the EEs. In this case, μ_i^*

is equal to the absolute value of μ_i. The reverse is also true; if $\mu_i^* = abs(\mu_i)$, the effects of the i^{th} parameter are monotonic.

The second proposed measure is the standard deviation of the EEs σ_i, which assesses the extent of interactions and non-linear effects of each input parameter i. This measure is defined as follows:

$$\sigma_i = \sqrt{\frac{1}{r-1}\sum_{t=1}^{r}(|EE_i^{*(t)}| - \mu_i^*)^2} \tag{36}$$

A graphical representation of the (μ_i^*, σ_i) points in the (μ^*, σ) plane allows a comparison of the sensitivities of different parameters taking into account at the same time the two sensitivity measures.

4.2. Latin Hypercube Sampling for Elementary Effects Method

Latin Hypercube Sampling (LHS) has become a popular technique for generating designs to computational experiments [38, 39]. To do that for the elementary effects method, three steps are essential: *(1)* The LHS generates $p = 2 \times r$ random samples of k uncorrelated parameters in the k-dimensional unit hypercube; where each component of $\boldsymbol{\theta}$ has an uniform distribution in the interval $[0, 1]$. *(2)* Returning to the specified distribution of the uncertain parameters by inverting the Cumulative Distribution Function (CDF). *(3)* Applying the One factor at a time strategy, which consists in adding the $r \times (k-1)$ points in order to establish r trajectories, each trajectory contains $k+1$ points. Therefore, the computational experiments matrix is composed of $r \times (k+1)$ random points of k uncorrelated parameters. Each row of the matrix is a point in the input space. The rows of the matrix are sorted in r blocks, each block includes $k+1$ rows (each block presents a trajectory). Inside each block, points differ only in one component at a time. Thus, each block allows to compute one Elementary Effect per input parameter.

Figure 4 shows an example of two parameters uniformly distributed in $[0\ 1]^2$ space. In order to determine 4 elementary effects per parameter, the LHS method generates 8 random points given in Figure 4.a. Adding 4 points whose one parameter changes at the time, provides 4 trajectories as shown in Figure 4.b. The LHS with the one factor at the time strategy ensure two levels per input parameter for one trajectory of the EEs method.

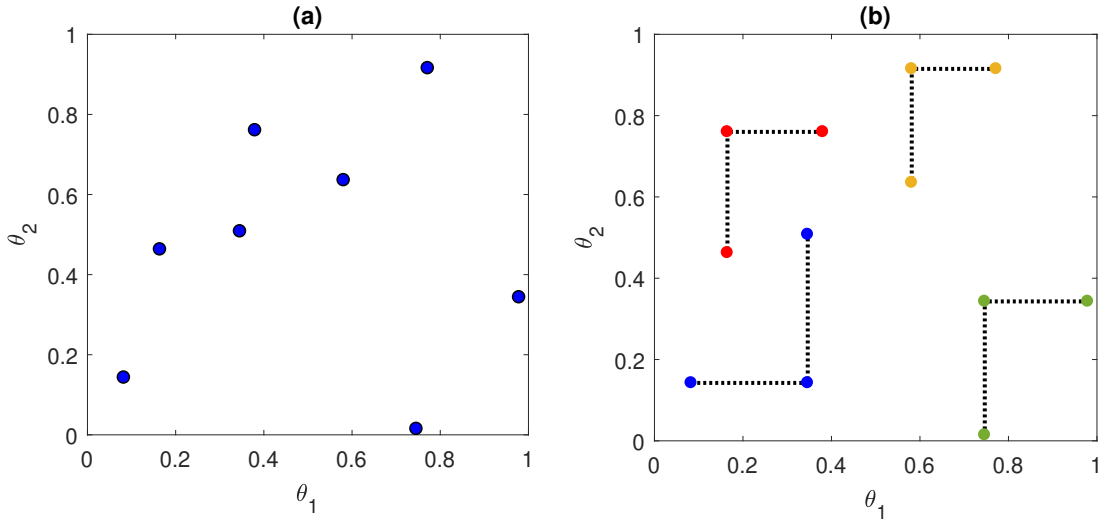

Figure 4: (a) Random points generated by the LHS method in two unit dimensions, (b) 4 trajectories in $[0\ 1]^2$ space for the EEs method

5. Numerical Example

This section presents a numerical example of the harvester introduced in Section 4, which is composed of two identical piezoceramic layers of PZT-5A bonded on the top and the bottom surfaces of an aluminum substrate. The geometrical dimensions and material properties of the harvester used in this example are given in Table 2 (adapted from Erturk and Inman [1]).

The ratio of the overhang length to the total thickness of the harvester is about 85.7, which makes it reasonable to neglect the shear deformation and the rotary inertia effects for the first few vibration modes. For the numerical simulation, we used modal mechanical damping ratios $\zeta_1 = 0.01$ and $\zeta_2 = 0.012$ for the first two modes. The proportional coefficients α and β given in Equation (18) are computed using these two damping ratios. The load resistance R is mounted in series with the piezoceramic layers as shown in Figure 2.

Table 2: Physical parameters values of the harvester structure of Fig.2

Parameters	Descriptions	Units[1]	PZT-5A	Aluminum
L	Beam length	mm	30	30
b	Beam width	mm	5	5
h_p , h_s	Layers thickness	mm	0.15	0.05
E_p , E_s	Young's modulus	GPa	61	70
ρ_p , ρ_s	Mass density	kg/m^3	7750	2700
e_{31}	Piezoelectric constant	C/m^2	-10.4	–
ϵ_{33}	Permittivity constant	nF/m	13.3	–

For the finite element discretization, the harvester is modeled in $1D$ using 30 linear elements with three degrees of freedom per node.

The model is validated for the frequency range from 0 to 5000 Hz by comparing the first three resonance frequencies computed by the finite element model to those given by the analytical solution computed by Erturk et Inman [1] for the same harvester for the short-circuit and open circuit

[1]Unit of parameter (PU), it will be used to define sensitivities units

conditions. The first three natural frequencies are listed in Table 3 with the effective electromechanical coupling factor k_{eff} defined in Equation (25) which is computed for the FE-model. We can notice that the natural frequencies for the open-circuit condition are higher than those obtained in the short-circuited case due to the electromagnetical coupling effects and the added stiffness in the open-circuit condition. Therefore, the natural frequencies for the two approaches are in excellent agreement for all modes. An infinitesimal error for the third mode can be due to the numerical computational errors caused by the approximation solution of the finite element method, which is so sensitive to the assigned discretization. These results confirm the validation of the finite element harvester model and allow for pursuing the study.

Table 3: The first three natural frequencies for the short circuit and open circuit conditions computed from the Finite Element Method (FE) and the Analytical solution (Anal.) [1]

.

Mode (r)	f_r^{cc} (FE)	f_r^{cc} (Anal. [1])	f_r^{co} (FE)	f_r^{co} (Anal. [1])	$k_{eff,r}$ (FE)
1	185.1	185.1	191.1	191.1	0.2561
2	1159.8	1159.7	1171.7	1171.6	0.1435
3	3246.7	3245.3	3258.2	3254.1	0.0845

The selected uncertain parameters are the Young modulus and the material densities for both the substrate and the piezoelectric layers, also the premittivity and piezoelectric constants for the piezoceramic layers. Table 4 lists the tolerances provided by the manufacturers as percent varation from the nominal values [11]. A tolerance of $\pm 20\%$ is reported for the piezoceramic PZT-5A electromechanical properties and $\pm 10\%$ for the Young's modulus

and density of the aluminum substrate material. An uniform distribution is assumed for all materials properties of the harvester.

Table 4: Bounds for the uniform PDF distribution associated to the electromechanical parameters; bounds are expressed in terms of the nominal values [11]

Parameters	Bounds
E_p	$\pm 20\%$
E_s	$\pm 10\%$
ρ_p	$\pm 20\%$
ρ_s	$\pm 10\%$
e_{31}	$\pm 20\%$
ϵ_{33}	$\pm 20\%$

The application of the Morris method for the voltage FRF of the bimorph piezoelectric energy harvester consists in computing $r = 10$ elementary effects for each parameter listed in table 4. Thus, 70 simulations are required for a fixed excitation frequency and load resistance. The aim of the study is to identify the effect of the excitation frequency on the importance order of the parameters particularly in the vicinity of the first mode. Furthermore, the system is be studied for both a short-circuit condition simulated using a load resistance $R = 100\ \Omega$ and an open-circuit condition simulated using for a load resistance $R = 10^7\ \Omega$.

Figure 5 shows the voltage and tip displacement FRFs responses of the harvester versus the excitation frequencies in the vicinity of the first mode for 70 samples. One can be observe the variability in the first natural frequency and in amplitude peaks. The voltage FRF peak varies between 0.02032 and 0.01152 V/g whereas the tip displacement FRF peak varies between 442.46

and 756.55 $\mu m/g$.

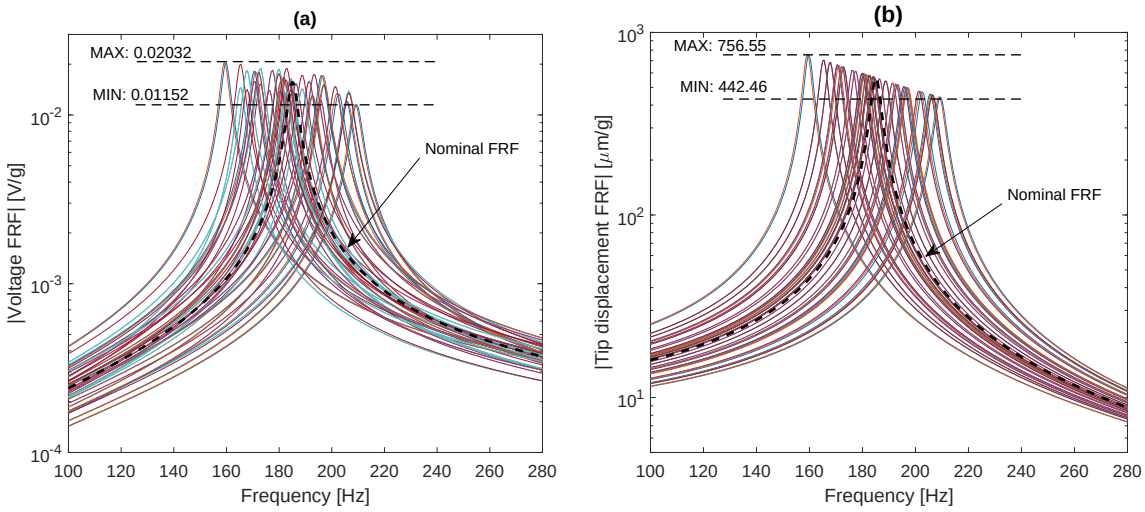

Figure 5: Modulus of FRFs versus excitation frequencies of the first mode for the 70 simulations of: (a) voltage and (2) Tip displacement for the short circuit condition $R = 100\Omega$

Figure 6 shows the average μ^* and the standard deviation σ of the EEs to the electromechanical characteristics of the bimorph piezoelectric energy harvester for the output voltage FRF at the selected excitation frequencies in the vicinity of the first natural frequency. The harvester has a 100 Ω load resistance connected in series between the two piezoelectric layers. One can notice that the hierarchical influence of the input parameters is unchangeable and independent of the excitation frequency. Moreover, the density and the elastic modulus of the piezoceramic layers have the highest values of the EEs indicators whereas the premittivity constant has the lowest values. These results provide a useful information about how significant uncertain parameters affect the output voltage of the harvester and how much

interaction exists between the parameters.

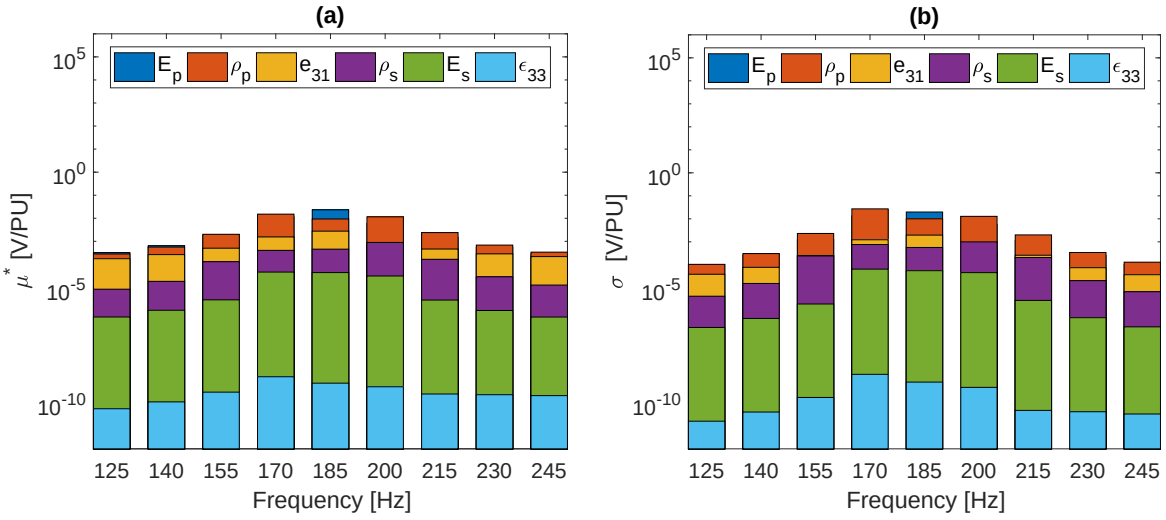

Figure 6: EEs measures for the voltage FRF of the bimorph piezoelectric energy harvester harvester for a load resistance $R = 100\ \Omega$ at excitation frequencies in the viscinity of the first natural frequency (a) the mean and (b) the standard deviation

Figure 7 shows the (μ^*, σ) scatter graph of the FRF voltage for the six parameters to the variation of the electromechanical characteristics for a load resistance $R = 100\ \Omega$ and and excitation frequency equal 185 Hz. The limits of the boxes correspond to a confidence interval of 95%. Clearly, we can see that the sensitivities of the absolute mean and standard deviation of the piezoelectric density ρ_p and the elastic modulus E_p are relatively significant compared to those of the piezoelectric constant, permittivity constant and substrate properties. Therefore, the density and elastic modulus of piezoelectric layers are the most important parameters that affect the output voltage FRF. Furthermore, the average and the standard deviation are of the same order of values. This means that the elastic modulus and

density of the piezoelectric layers are strongly influenced by the nonlinear effects and interactions with others parameters.

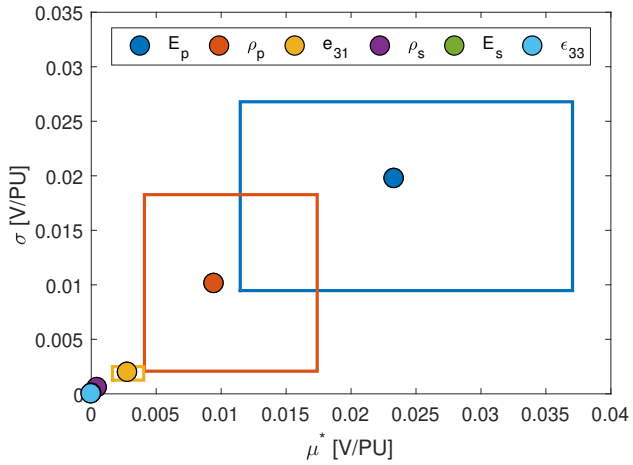

Figure 7: (μ^*, σ) Scatter graph of the voltage FRF for bimorph piezoelectric energy harvester harvester for a load resistance $R = 100\ \Omega$ and an excitation frequency 185 Hz with 95% confidence interval

Considering next the sensitivity analysis for a roughly open circuit condition depicted by a load resistance $R = 10^7\ \Omega$. Figure 8 shows the average μ^* and the standard deviation σ of the EEs for the output voltage FRF at a set of excitation frequencies in the vicinity of first natural frequency. One can notice the EEs sensitivity measures are in the same order for all considered frequencies. This means that the parameters importance is the same for any of the excitation frequency. However, the order influence of the parameters change form the short to the open circuit condition. The influence of the permittivity constant becomes higher than the Aluminum substrate material properties. The density and the elastic modulus of the piezoceramic layers remain the highest EEs indicators similarly to the case

of a roughly closed circuit whereas the EEs indicators for the aluminum properties become the lowest.

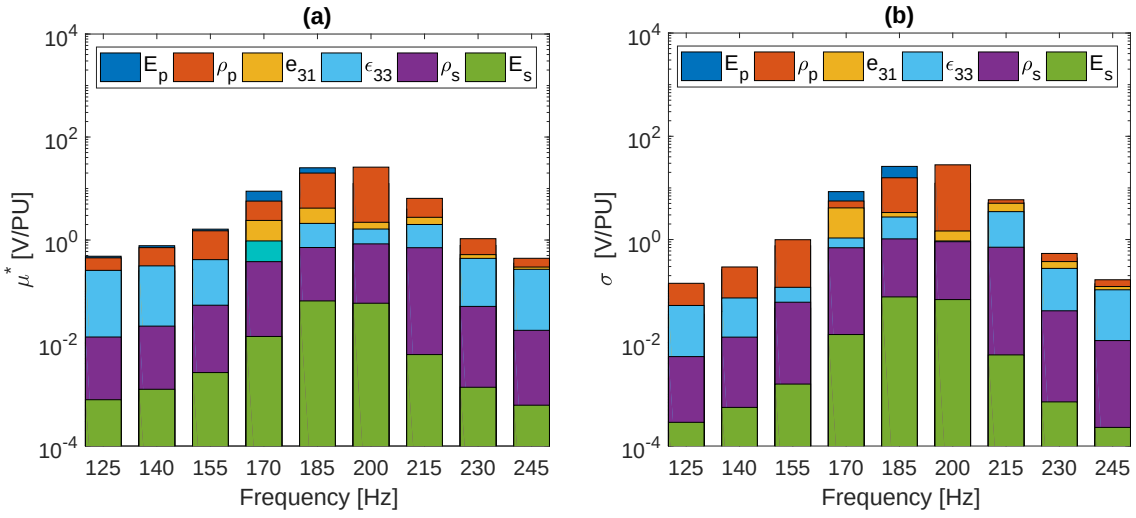

Figure 8: EEs measures for the voltage FRF of the bimorph piezoelectric energy harvester harvester for a load resistance $R = 10^7\ \Omega$ at excitation frequencies in the viscinity of the first natural frequency (a) the mean and (b) the standard deviation

Figure 9 presents the standard deviation versus the absolute mean of the EEs and the confidence interval of 95% for the k electromechanical characteristics of the harvester for the case of a roughly open circuit condition depicted by a load resistance $R = 10^7\ \Omega$ and for an excitation frequency of 185 Hz. One can clearly notice that the piezoelectric density and elastic modulus remain the major contributors for the uncertainty of the voltage FRF. The premittivity constant becomes more significant compared to the Aluminum substrate characteristics which have negligible effect on the harvester voltage response in both short and open circuit.

In order to evaluate the harvester performance, The EEMCF defined in

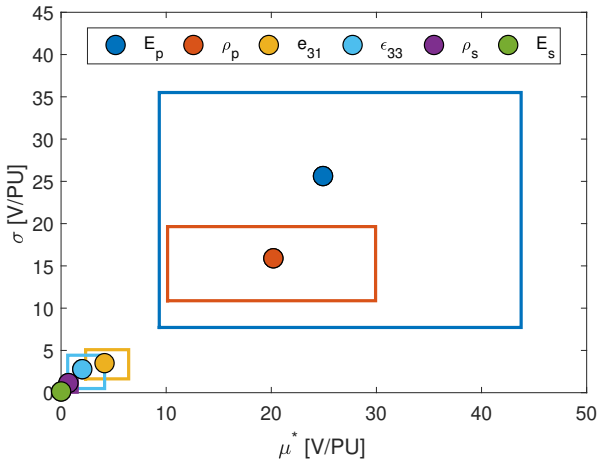

Figure 9: (μ^*, σ) Scatter graph of the voltage FRF for the bimorph piezoelectric energy harvester harvester for a load resistance $R = 10^7\ \Omega$ and excitation frequency 185 Hz with 95% confidence interval

(30) as the ratio of the exchanged mechanical energy and electrical energies is shown in Figure 10 for each of the 10 electromechanical characteristic sample vectors used in this GSA study. One can observe that the EEMCF can reach a maximum value of 0.34 for the 42^{th} sample vector. This results can be very useful for the research of optimal harvester parameters that maximize this factor.

6. Conclusion

In this paper, a finite element formulation of the electromechanical coupling problem for a laminated piezoelectric cantilever beam introduced. The finite element formulation is applied in the case of a symmetric bimorph piezoelectric energy harvester. The FRFs of the harvester are used as the performance predictors. The Morris global sensitivity method using the el-

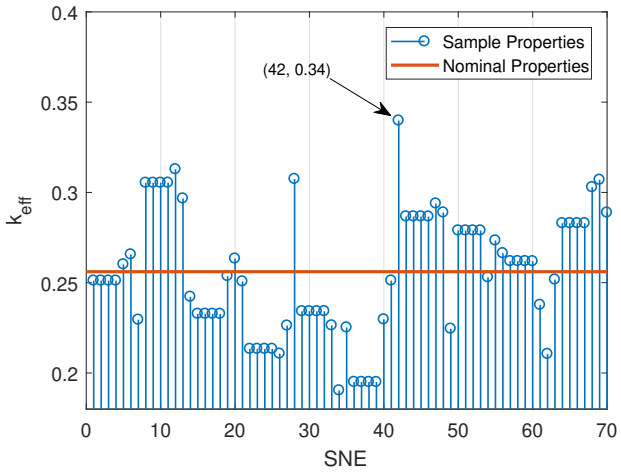

Figure 10: The EEMCF k_{eff} for the 70 simulations used in the GSA

ementary effects is used to study the effect of the variability of the material properties of the substrate and piezoelectric layers on the voltage FRF output of the harvester. The EEs method can estimate the effect of parameters and their interactions by considering both the mean and the variance of the elementary effects. Using only 70 simulations, the sensitivities measures show that the piezoelectric elastic modulus and its density are the most influential parameters on the voltage FRF. These results are in agreement with the published research of Ruiz et al [11] which used the Sobol' indices as a variance based sensitivity analysis method. The method of Morris correctly screens the most and least sensitive parameters among few selected parameters for a spatially distributed bimorph piezoelectric energy harvester FE-model with fewer model evaluations than the Sobol's method.

Future research may consider second order sensitivity analysis using the elementary effects method to minutely study the interactions between pa-

rameters properties of the harvester.

References

[1] A. Erturk, D. J. Inman, Piezoelectric energy harvesting, Wiley, Chichester, 2011, oCLC: ocn687714431.

[2] A. Erturk, D. J. Inman, A Distributed Parameter Electromechanical Model for Cantilevered Piezoelectric Energy Harvesters, Journal of Vibration and Acoustics 130 (4) (2008) 041002. doi:10.1115/1.2890402.

[3] C. De Marqui Junior, A. Erturk, D. J. Inman, An electromechanical finite element model for piezoelectric energy harvester plates, Journal of Sound and Vibration 327 (1-2) (2009) 9–25.

[4] M. Rosa, C. De Marqui Junior, Modeling and Analysis of a Piezoelectric Energy Harvester with Varying Cross-Sectional Area, Shock and Vibration 2014 (2014) 1–9. doi:10.1155/2014/930503.

[5] M. Lasecka Plura, R. Lewandowski, Design sensitivity analysis of frequency response functions and steady state response for structures with viscoelastic dampers, Vibrations in Physical Systems 26.

[6] A. d. Lima, A. Faria, D. Rade, Sensitivity analysis of frequency response functions of composite sandwich plates containing viscoelastic layers, Composite Structures 92 (2) (2010) 364–376. doi:10.1016/j.compstruct.2009.08.017.

[7] F. Campolongo, A. Saltelli, J. Cariboni, From screening to quantitative sensitivity analysis. A unified approach, Computer Physics Communications 182 (4) (2011) 978–988. doi:10.1016/j.cpc.2010.12.039.

[8] R. Sharp, P. Brooks, Sensitivities of frequency response functions of linear dynamic systems to variations in design parameter values, Journal of Sound and Vibration 126 (1) (1988) 167–172. doi:10.1016/0022-460X(88)90406-3.

[9] A. M. G. de Lima, M. H. Stoppa, D. A. Rade, V. Steffen Jr, Sensitivity analysis of viscoelastic structures, Shock and Vibration 13 (4-5) (2006) 545–558.

[10] T. H. Ng, W. H. Liao, Sensitivity Analysis and Energy Harvesting for a Self-Powered Piezoelectric Sensor, Journal of Intelligent Material Systems and Structures 16 (10) (2005) 785–797. doi:10.1177/1045389X05053151.

[11] R. O. Ruiz, V. Meruane, Uncertainties propagation and global sensitivity analysis of the frequency response function of piezoelectric energy harvesters, Smart Materials and Structures 26 (6) (2017) 065003. doi:10.1088/1361-665X/aa6cf3.

[12] P. Peralta, R. O. Ruiz, V. Meruane, Bayesian Framework to Quantify Uncertainties in Piezoelectric Energy Harvesters, Proceedings of the ASME 2018 V001T04A002 (40795) (2018) V001T04A002. doi:10.1115/VVS2018-9318.

[13] F. Pianosi, F. Sarrazin, T. Wagener, A Matlab toolbox for Global Sensitivity Analysis, Environmental Modelling & Software 70 (2015) 80–85. doi:10.1016/j.envsoft.2015.04.009.

[14] W. Chen, R. Jin, A. Sudjianto, Analytical Variance-Based Global Sensitivity Analysis in Simulation-Based Design Under Uncertainty, Jour-

nal of Mechanical Design 127 (5) (2004) 875–886. doi:10.1115/1.1904642.

[15] S. Kucherenko, M. Rodriguez-Fernandez, C. Pantelides, N. Shah, Monte Carlo evaluation of derivative-based global sensitivity measures, Reliability Engineering & System Safety 94 (7) (2009) 1135–1148. doi:10.1016/j.ress.2008.05.006.

[16] M. D. Morris, Factorial sampling plans for preliminary computational experiments, Technometrics 33 (2) (1991) 161–174.

[17] D. Garcia Sanchez, B. Lacarrière, M. Musy, B. Bourges, Application of sensitivity analysis in building energy simulations: Combining first- and second-order elementary effects methods, Energy and Buildings 68 (2014) 741–750. doi:10.1016/j.enbuild.2012.08.048.

[18] I. Sobol', Global sensitivity indices for nonlinear mathematical models and their Monte Carlo estimates, Mathematics and Computers in Simulation 55 (1-3) (2001) 271–280. doi:10.1016/S0378-4754(00)00270-6.

[19] A. Saltelli, P. Annoni, I. Azzini, F. Campolongo, M. Ratto, S. Tarantola, Variance based sensitivity analysis of model output. Design and estimator for the total sensitivity index, Computer Physics Communications 181 (2) (2010) 259–270. doi:10.1016/j.cpc.2009.09.018.

[20] J. D. Herman, J. B. Kollat, P. M. Reed, T. Wagener, Technical Note: Method of Morris effectively reduces the computational demands of global sensitivity analysis for distributed watershed models, Hydrology

and Earth System Sciences 17 (7) (2013) 2893–2903. doi:10.5194/hess-17-2893-2013.

[21] F. Campolongo, J. Cariboni, A. Saltelli, An effective screening design for sensitivity analysis of large models, Environmental Modelling & Software 22 (10) (2007) 1509–1518. doi:10.1016/j.envsoft.2006.10.004.

[22] Y. Amini, H. Emdad, M. Farid, Finite element modeling of functionally graded piezoelectric harvesters, Composite Structures 129 (2015) 165–176.

[23] O. Thomas, J.-F. Deü, J. Ducarne, Vibrations of an elastic structure with shunted piezoelectric patches: efficient finite element formulation and electromechanical coupling coefficients, International Journal for Numerical Methods in Engineering 80 (2) (2009) 235–268. doi:10.1002/nme.2632.

[24] W. Larbi, J.-F. Deü, R. Ohayon, Finite element formulation of smart piezoelectric composite plates coupled with acoustic fluid, Composite Structures 94 (2) (2012) 501–509. doi:10.1016/j.compstruct.2011.08.010.

[25] Y. C. Shu, I. C. Lien, W. J. Wu, An improved analysis of the SSHI interface in piezoelectric energy harvesting, Smart Materials and Structures 16 (6) (2007) 2253–2264. doi:10.1088/0964-1726/16/6/028.

[26] W. Larbi, J.-F. Deü, R. Ohayon, R. Sampaio, Coupled FEM/BEM for control of noise radiation and sound transmission using piezoelectric

shunt damping, Applied Acoustics 86 (2014) 146–153. doi:10.1016/j.apacoust.2014.02.003.

[27] J. S. Moita, A. L. Araújo, V. F. Correia, C. M. Mota Soares, J. Herskovits, Active-passive damping in functionally graded sandwich plate/shell structures, Composite Structures 202 (2018) 324–332. doi:10.1016/j.compstruct.2018.01.089.

[28] W. Larbi, J.-F. Deü, Reduced order finite element formulations for vibration reduction using piezoelectric shunt damping, Applied Acousticsdoi:10.1016/j.apacoust.2018.04.016.

[29] M. Trindade, A. Benjeddou, Effective Electromechanical Coupling Coefficients of Piezoelectric Adaptive Structures: Critical Evaluation and Optimization, Mechanics of Advanced Materials and Structures 16 (3) (2009) 210–223. doi:10.1080/15376490902746863.

[30] W. Larbi, J.-F. Deü, M. Ciminello, R. Ohayon, Structural-Acoustic Vibration Reduction Using Switched Shunt Piezoelectric Patches: A Finite Element Analysis, Journal of Vibration and Acoustics 132 (5) (2010) 051006. doi:10.1115/1.4001508.

[31] L. Pereira da Silva, W. Larbi, J.-F. Deü, Topology optimization of shunted piezoelectric elements for structural vibration reduction, Journal of Intelligent Material Systems and Structures 26 (10) (2015) 1219–1235. doi:10.1177/1045389X14538533.

[32] S. R. Anton, A. Erturk, D. J. Inman, Multifunctional Unmanned Aerial Vehicle Wing Spar for Low-Power Generation and Storage, Journal of Aircraft 49 (1) (2012) 292–301. doi:10.2514/1.C031542.

[33] R. Aloui, W. Larbi, M. Chouchane, Sensitivity analysis of frequency response functions for load resistance of piezoelectric energy harvesters, in: T. Fakhfakh, C. Karra, S. Bouaziz, F. Chaari, M. Haddar (Eds.), Advances in Acoustics and Vibration II, Springer International Publishing, Cham, 2019, pp. 136–148.

[34] M. D. Morris, T. J. Mitchell, Exploratory designs for computational experiments, Journal of Statistical Planning and Inference 43 (3) (1995) 381 – 402. doi:doi.org/10.1016/0378-3758(94)00035-T.

[35] D. M. Hamby, A review of techniques for parameter sensitivity analysis of environmental models, Environmental Monitoring and Assessment 32 (2) (1994) 135–154. doi:10.1007/BF00547132.

[36] J. R. F. Arruda, J. M. C. Santos, Mechanical Joint Parameter Estimation Using Frequency Response Functions and Component Mode Synthesis, Mechanical Systems and Signal Processing 7 (1993) 493–508.

[37] A. Saltelli (Ed.), Global sensitivity analysis: the primer, Wiley, Chichester, 2008, oCLC: 254420563.

[38] T. Andres, Sampling methods and sensitivity analysis for large parameter sets, Journal of Statistical Computation and Simulation 57 (1-4) (1997) 77–110. doi:10.1080/00949659708811804.

[39] M. Stein, Large sample properties of simulations using latin hypercube sampling, Technometrics 29 (2) (1987) 143–151. doi:10.1080/00401706.1987.10488205.